ELECTROCHEMISTRY

Composite lithium electrode with mesoscale skeleton via simple mechanical deformation

Zheng Liang[1], Kai Yan[1], Guangmin Zhou[1], Allen Pei[1], Jie Zhao[1], Yongming Sun[1], Jin Xie[1], Yanbin Li[1], Feifei Shi[1], Yayuan Liu[1], Dingchang Lin[1], Kai Liu[1], Hansen Wang[1], Hongxia Wang[1], Yingying Lu[1], Yi Cui[1,2]*

Lithium metal–based batteries are attractive energy storage devices because of high energy density. However, uncontrolled dendrite growth and virtually infinite volume change, which cause performance fading and safety concerns, have limited their applications. Here, we demonstrate that a composite lithium metal electrode with an ion-conducting mesoscale skeleton can improve electrochemical performance by locally reducing the current density. In addition, the potential for short-circuiting is largely alleviated due to side deposition of mossy lithium on the three-dimensional electroactive surface of the composite electrode. Moreover, the electrode volume only slightly changes with the support of a rigid and stable scaffold. Therefore, this mesoscale composite electrode can cycle stably for 200 cycles with low polarization under a high areal current density up to 5 mA/cm^2. Most attractively, the proposed fabrication process, which only involves simple mechanical deformation, is scalable and cost effective, providing a new strategy for developing high performance and long lifespan lithium anodes.

INTRODUCTION

Given their high specific capacity, low atomic weight, and low anode potential, next-generation secondary batteries based on lithium (Li) metal anodes could store electrochemical energy better than currently existing commercial Li ion batteries (*1*–*7*). However, the formation of ramified dendritic Li during cycling challenges the development of a practical Li metal battery. Consequences of this Li dendrite growth include internal short circuits from sharp Li dendrite penetration and poor electrochemical performance due to intensive side reactions and solid electrolyte interphase (SEI) formation (*5*, *7*–*11*). Many strategies have been proposed and demonstrated to eliminate the aforementioned intrinsic problems of Li anodes (*12*–*23*). Our group, in particular, has placed substantial effort in building a host for Li by fabricating composite Li electrodes. Several designs for Li encapsulation inside a scaffold have been proposed (*21*, *24*–*29*), and a number of other research groups have also demonstrated the progress of the host designs (*30*–*35*); examples of these designs include guided nucleation (*21*, *31*), guided growth (*20*, *24*, *32*), and more recent melt-infusion methods (*25*–*30*, *34*, *35*). These strategies can ensure the suitable encapsulation of Li within a scaffold and thus enable a high electroactive area, improved electrochemical performance, and minimal volume change. Nevertheless, these methods require high-cost and complicated fabrication procedures. A multistep nanosynthesis is involved in guided nucleation with prestored gold nanoparticles as nucleation seeds (*21*). High temperatures over 200°C and safety precautions are required for Li melt-infusion (*25*–*27*). The highly complex fabrication and processing in these techniques require further development in their practical application, and as such, a simple yet effective method to build a host for Li is in high demand.

Here, we report a newly developed composite Li metal anode fabricated via a simple rolling-cutting method. In contrast to our previous designs that require chemical processes, this composite Li anode only involves mechanical deformation. As schematically illustrated in Fig. 1A, a thin layer of nanoporous polyethylene (PE) film (~12 μm) was placed on the top surface of a layer of Li foil (~50 to 60 μm). The two layers of material were pressed tightly to ensure tight and smooth contact. Afterward, the double-layer strip was rolled into a cylinder manually (Fig. 1B). The cross-sectional area of the cylinder could be tuned by controlling the total length of the double-layer strip. The as-made cylinder was then cut into round disks using a sharp blade (Fig. 1B). Keeping the same geometric dimensions as typical Li metal foil electrodes, the area of each round disk is fixed to be 1 cm^2 with a thickness of around 1 mm. With this design, the porous PE film

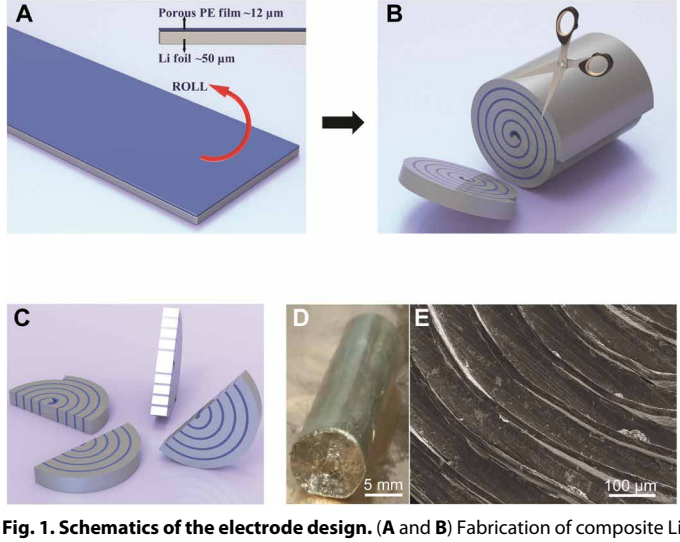

Fig. 1. Schematics of the electrode design. (**A** and **B**) Fabrication of composite Li electrode via mechanical deformation. (**C**) Tilted view of the resulting composite electrode disk showing alternating building blocks of Li strip and porous PE film. (**D**) Digital photo image of the composite Li electrode. Photo credit: Zheng Liang, Stanford University. (**E**) SEM image of the composite Li electrode.

[1]Department of Materials Science and Engineering, Stanford University, Stanford, CA 94305, USA. [2]Stanford Institute for Materials and Energy Sciences, SLAC National Accelerator Laboratory, 2575 Sand Hill Road, Menlo Park, CA 94025, USA.
*Corresponding author. Email: yicui@stanford.edu

can be uniformly embedded between Li layers, thus forming a well-defined lamellar structure with alternating blocks of Li and porous PE (Fig. 1C). The cross section of the rolled cylinder can be observed in Fig. 1D, exhibiting a flat, smooth surface after blade cutting. Scanning electron microscopy (SEM) demonstrates the designed spiral shape, showing the closely packed layers (Fig. 1E). According to Fig. 1 (D and E), minimal structure breakage and discontinuity of the Li within the composite electrode can be observed after the facile mechanical processing of the soft, ductile Li strip. During the subsequent experiments and measurements, liquid electrolyte can wet and infiltrate the entire porous PE film. Consequently, electrochemical processes can take place on the sidewalls of the Li strips, thus causing "side deposition." The enlarged electroactive surface area of our as-prepared composite electrode reduces local current density effectively (*36*). On one hand, it is widely accepted that the formation of mossy Li is enhanced by high applied areal current density for Li deposition and extraction (*8*, *36*, *37*), while a high electroactive surface area brings a lower actual current density, thus alleviating Li dendrite formation (*1*, *36*, *38*, *39*). On the other hand, high electroactive surface area of Li electrodes triggers intense side reactions and SEI formation, which account for the typical electrochemical performance decay (*36*). Under these circumstances for a balance, attempts have been made to increase the electroactive area at a moderate level. The thickness of both the Li foil and porous PE film in our design are in the micrometer scale. Therefore, the electroactive surface area and related side reactions are well controlled compared with previous examples with nanoscale conducting matrices.

In summary, the motivation for this work is to build a mesoscale conductive matrix for Li metal anodes. The resulting composite Li anode exhibits improved electrochemical performance and mitigated dendrite formation due to locally reduced Li plating/stripping current density. The risk of internal short-circuiting through mossy Li penetration is lowered by the side deposition effect, thereby facilitating safe battery cycling. Furthermore, the presence of a rigid scaffold maintains a relatively constant electrode shape and volume during cycling, which, again, reinforces the safety and stability of the battery. Because Li is ductile and soft in nature, this mechanical processing is simple and low cost, providing a new concept and strategy for constructing composite Li electrodes.

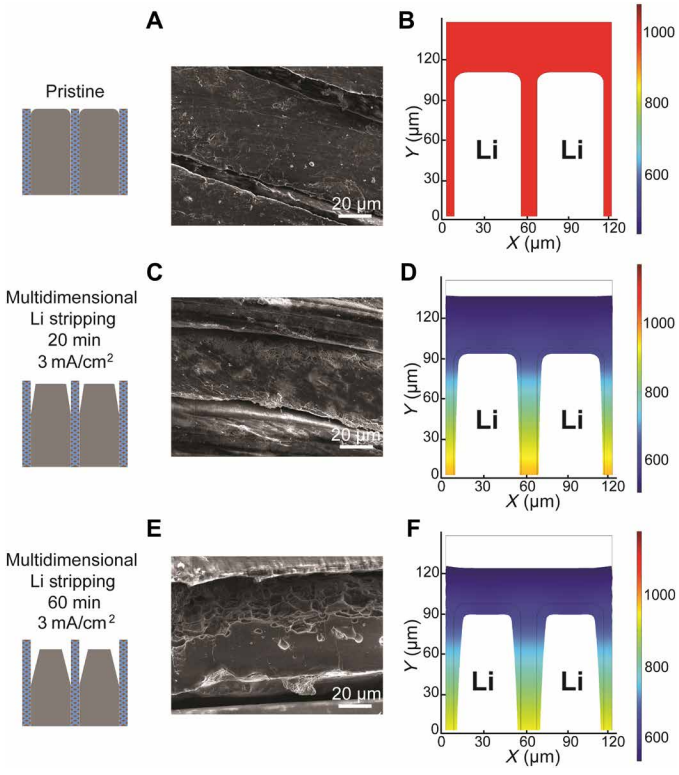

Fig. 2. COMSOL multiphysics modeling of composite electrode geometry during Li stripping. (**A**) Schematic and top-view SEM image of the composite electrode at the initial stage and (**B**) corresponding initial state of the model. (**C**) Top-view SEM image of the composite electrode after stripping 1 mAh/cm^2 of Li under a current density of 3 mA/cm^2 and (**D**) corresponding slightly stripped model. (**E**) Top-view SEM image of the composite electrode after stripping 3 mAh/cm^2 Li under a current density of 3 mA/cm^2 and (**F**) corresponding increasingly stripped model. In the COMSOL modeling part, the width of each Li strip and PE film is around 50 and 12 μm, respectively, and the color scale represents the local Li^+ ion concentration in millimolar (mM). Additional simulation parameters are available in the Supplementary Materials.

RESULTS AND DISCUSSION

Li plating/stripping behaviors on the composite Li electrode

The composite Li electrode is expected to exhibit electrochemical activity at both the top surface and sidewalls, enabling three-dimensional Li plating/stripping. To confirm this concept, we conducted both SEM study and COMSOL simulation. Figure 2 displays the actual shape and corresponding simulated shape of this composite Li electrode during various stages in a simple Li stripping process. The mesoscale composite Li electrode was subjected to an electrochemical Li extraction under a constant areal current density of 3 mA/cm^2. The pristine electrode shows a flat top surface and tight packing of the Li strip and PE film (Fig. 2A). The white regions in Fig. 2 (B, D, and F) represent the Li strips, while the colored regions represent the Li^+ ion concentration in the surrounding electrolyte. In the following stripping process, both height and width of the Li strip decrease, suggesting a three-dimensional plating/stripping (Fig. 2, C and E). The corresponding modeling confirms this shape change during Li stripping (Fig. 2, D and F). Obviously, the Li strip width decreases more rapidly on the top part than the bottom, thereby forming a structure with a trapezoidal cross section. This fact implies that the top part of the composite electrode has much higher electrochemical activity than the part deep inside due to the limitation of Li ion diffusion (*25*–*27*).

To evaluate the influence of Li strip thickness on the cycling behavior of the composite electrode, we fabricated various composite Li electrodes using Li foils with three thicknesses (50, 380, and 750 μm). The processing methods were the same for all the electrodes, and the corresponding morphologies were studied in fig. S1 (A to C). The composite electrode disks with various Li foils have the same diameter and thickness for comparison. Symmetric cells were constructed and subjected to Li plating/stripping processes with current densities of 1, 3, and 5 mA/cm^2 for a total of 1 mAh/cm^2. Voltage profiles at selected cycles are presented in fig. S1 (D to L). Composite electrodes with 50-μm-thick Li foil display superior cycling behavior with small polarization and flat voltage plateaus. This behavior is attributed to the fact that the composite electrode with the thinnest Li foil obtains the largest enhancement in electroactive surface area. In the following experiments, the composite electrodes tested are the electrodes using Li foil with a thickness of 50 μm.

Electrochemical performance evaluation of the composite Li electrode

To study the electrochemical performance of the composite Li electrode, we constructed symmetric cells using two identical composite electrodes with 50-μm-thick Li. Moreover, we used a fixed amount of electrolyte (200 μl) for all tests to ensure a fair comparison. Figure 3A shows the voltage profiles of the Li plating/stripping process at various current densities for cells with bare (control) and composite Li electrodes (spiral Li-50). The symmetric cell using composite electrodes shows a flat and stable voltage plateau with a smaller absolute overpotential value than that of the cell with control electrodes. This observation can be attributed to the fact that the electroactive surface area for composite electrodes is much larger under the same geometric dimensions (*25*). Consequently, the charge transfer resistance and polarization at the interface in the composite Li electrodes are reduced when the same amount of current is applied (*40*, *41*). The corresponding voltage hysteresis, defined as the sum of Li deposition and Li stripping extraction overpotential, is plotted versus cycling

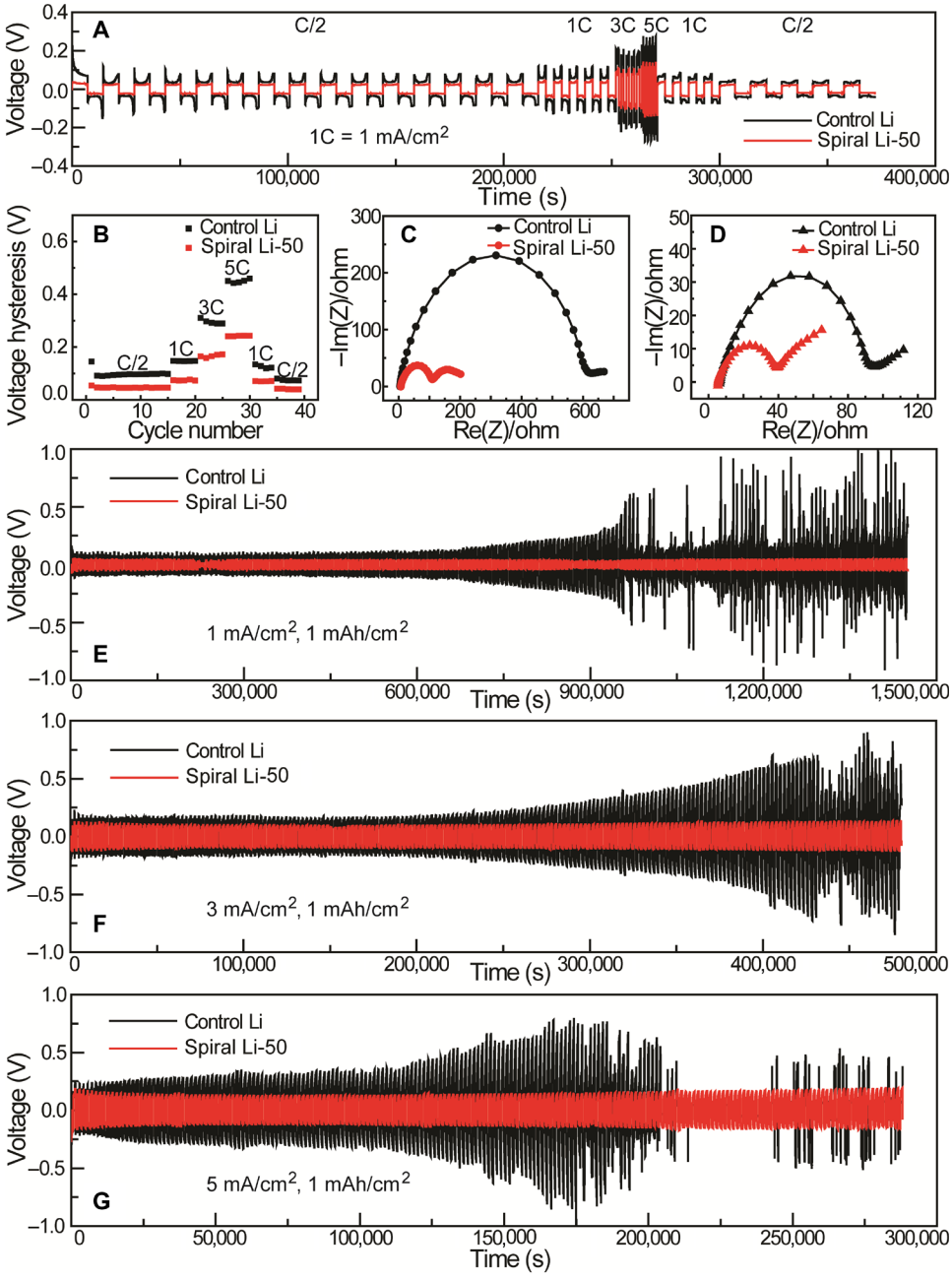

Fig. 3. Electrochemical performances of symmetric cells using control Li and composite Li electrodes. (**A**) Comparison of voltage profiles and (**B**) the corresponding hysteresis for cells using control and composite electrodes during Li plating/stripping processes under various current rates ranging from C/2 to 5C, where 1C is 1 mA/cm^2. (**C**) Impedance spectroscopy of cells with control and composite electrodes before cycling and (**D**) after the first cycle. (**E** to **G**) Long-term cycling of control Li and composite Li symmetric cells with current densities of 1, 3, and 5 mA/cm^2 and a deposition/stripping capacity of 1 mAh/cm^2.

numbers, as presented in Fig. 3B. The symmetric cell with a composite electrode exhibits a steadily increasing hysteresis of 46, 73, 166, and 241 mV at C/2, C, 3C, and 5C, respectively. Meanwhile, the cell using a control electrode shows increased values of 98, 146, 295, and 450 mV under the same test conditions. The excellent rate capability of composite Li electrodes again confirms the beneficial effects of high surface area on galvanostatic cycling behavior. We also measured electrochemical impedance spectra (EIS) of bare and composite Li electrodes in a symmetric cell configuration, as shown in Fig. 3 (C and D). The interfacial impedance values for bare and composite Li electrodes before cycling, as indicated by the high frequency semicircle, are ~580 and ~100 ohm (Fig. 3C), which respectively decrease to ~90 and ~45 ohm after the first cycle (Fig. 3D). Symmetric cells with the composite electrode exhibit much smaller overall impedance compared to those with bare Li electrodes. This result implies that the increase in electroactive surface area increases electrochemical reaction rate and improves charge transfer kinetics (*42*). Long-term symmetric cycling results of the control and composite electrodes with constant areal capacity of 1 mAh/cm^2 are shown in Fig. 3 (E to G). We conducted the test under various current densities of 1, 3, and 5 mA/cm^2. Symmetric cells using control Li electrodes exhibit gradually increasing polarization until an abrupt voltage drop, thus implying an uncontrolled Li dendrite growth, followed by internal short-circuiting (*19*, *43*). This change mainly originates from the fluctuating electrode shape/volume during a hostless deposition/extraction of bare Li foil (*44*). However, symmetric cells using composite electrodes can cycle stably for over 200 cycles under high current densities up to 5 mA/cm^2 with no evidence of dendrite-induced failure (Fig. 3G). These results indicate that ramified Li dendrite formation is lessened because of the reduced local current density and the presence of a stable scaffold (*45*).

To show the effectiveness of the ion-conducting matrix, we prepared composite Li electrodes with Li embedded in nonporous PE film for comparison (fig. S2). The dense composite electrode has the same geometric dimension as the porous composite electrode. The nonporous PE film has no electrolyte permeability; therefore, it is not a conductor of Li ions. As a result, this dense composite Li electrode only exhibits electrochemical activity at the top surface, which can be confirmed by the shape change during an electrochemical Li stripping process, as presented in fig. S3. The porous composite electrode exhibits changes in width and height, thus forming a shape with a trapezoidal cross section (fig. S3A). By contrast, the composite electrode with dense nonporous PE film shows dimension change only in height (fig. S3B). Furthermore, as shown in fig. S4, no noticeable enhancement in cycling stability is observed for a composite Li electrode with nonporous PE films under various current densities. Apparently, the aforementioned improvement in electrochemical performance in Fig. 3 results from the electroactive sidewalls of the composite electrode. With liquid electrolyte accessible along electrode sidewalls, the local current density is considerably reduced, and the electrochemical performance is improved (*43*).

Full cells consisting of Li cobalt oxide (LCO) and a Li metal electrode were assembled to investigate the battery performance under practical applications. We evaluated the rate capability of the cells via cycling at rates ranging from C/5 to 5C, as presented in Fig. 4A. The full cell using the composite Li electrode delivers reversible

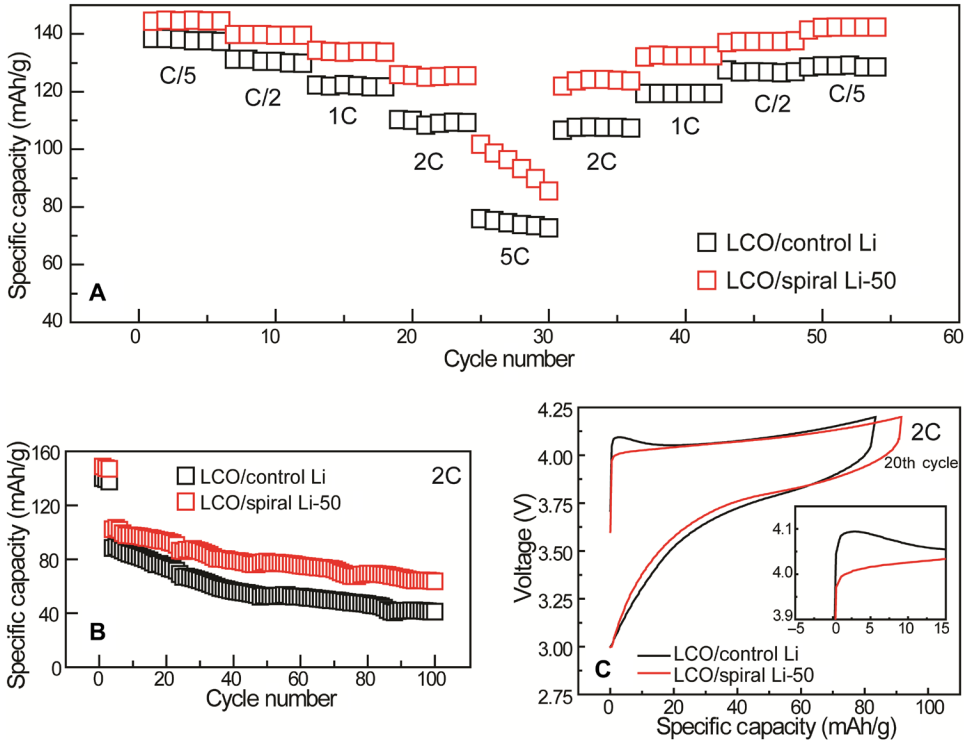

Fig. 4. Electrochemical performance of LCO full cells using control Li and composite Li electrodes. (**A**) Rate capability of a LCO/control Li cell and a LCO/spiral Li-50 cell under various current densities from C/5 to 5C. (**B**) Long-term cycling of a LCO/Control Li cell and a LCO/spiral Li-50 cell at 2C. The full cell was first activated at a low rate of C/5 for 3 cycles. (**C**) Voltage profiles of a LCO/control Li cell and a LCO/spiral Li-50 cell at a current rate of 2C at the 20th cycle. The inset is enlarged voltage curve at initial charging stage.

discharge capacity of 144, 139, 133, 125, and 98 mAh/g at C/5, C/2, C, 2C, and 5C, respectively. The capacity almost returns to the original value when the rate is recovered to C/5. In contrast, the full cell with the control Li electrode exhibits fast capacity decay as the current rate increases, and this difference in discharge capacities becomes more remarkable with increasing current density (Fig. 4A). Moreover, the cycling stability of full cells was studied at room temperature and 2C rate (1.28 mA/cm^2). The cell using a composite Li electrode displays superior cycling stability and improved discharge capacity retention (62% retention after 100 cycles for composite electrode) compared to the cell using a control electrode (46% retention after 100 cycles for control electrode) as shown in Fig. 4B. The remarkable rate capability and cycling retention of the composite electrode confirm a stable Li electrode with locally reduced current density and a supporting skeleton (*25*). Figure 4C presents the voltage profiles for cells with a control and composite electrodes at the 20th cycle. The cell polarization for the control electrode is much larger compared with that for the composite electrode, originating from the large charge transfer resistance, in good agreement with the EIS results (*46*). In addition, irregular voltage variation with spikes can be noticed for the control electrode at the initial charging stage, indicating an unstable electrode surface (*25*, *43*).

Structural stability of the composite Li electrode

We performed SEM characterization on cycled composite electrodes to examine the structural stability of composite Li electrodes after cycling. For composite electrodes after 10 and 100 cycles, as shown in Fig. 5 (B and C), the well-defined lamellar structure and close-packed pattern are well preserved compared with the pristine electrode in Fig. 5A. The intactness of the structure indicates that the composite electrode can tolerate the large shape/volume change during Li plating/stripping process with an areal capacity of 1 mAh/cm^2. In Fig. 5B, the boundary of Li in contact with PE films slowly becomes a porous structure (light region in Fig. 5B). This result suggests that

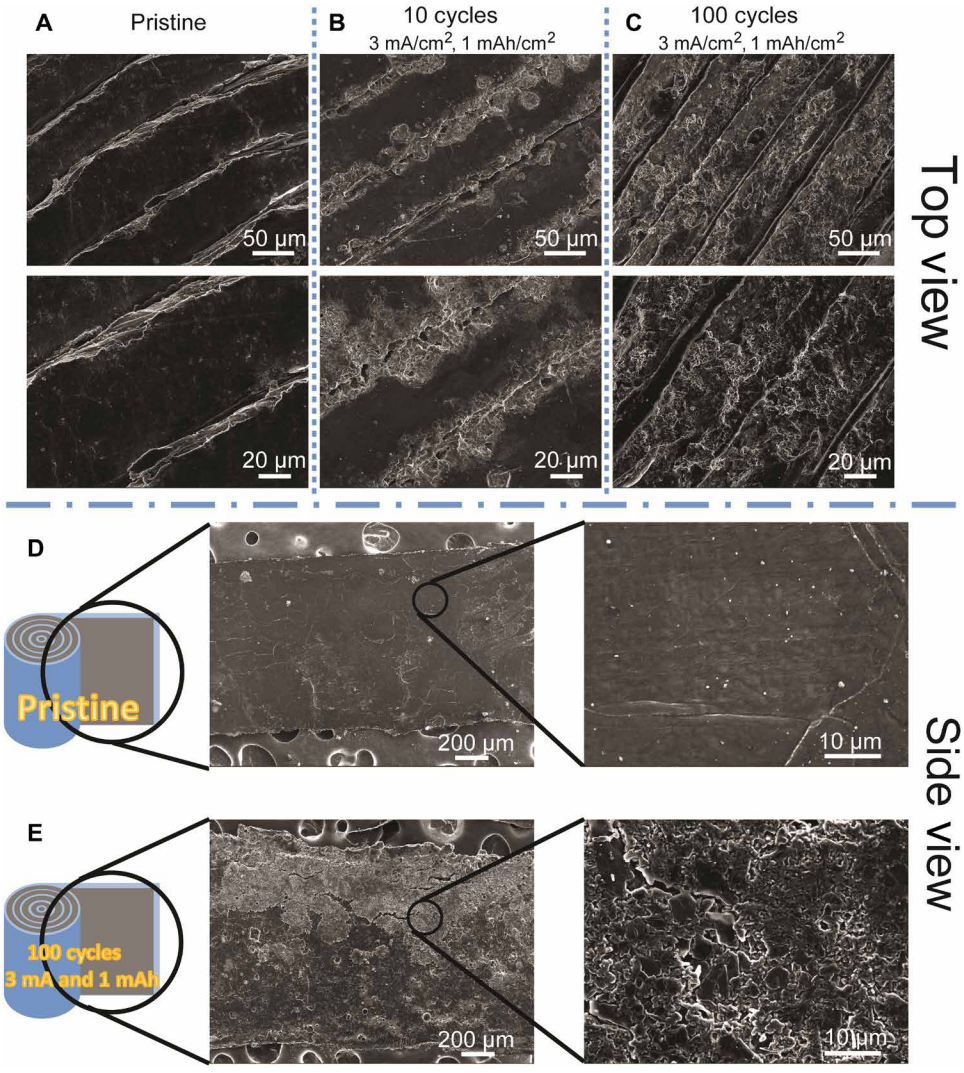

Fig. 5. SEM images of the pristine and cycled composite Li electrode. (**A**) Top-view SEM images of the pristine composite Li electrode. (**B**) Top-view SEM images of the composite Li electrode after 10 cycles at 3 mA/cm^2 for a total of 1 mAh/cm^2. (**C**) Top-view SEM images of the composite Li electrode after 100 cycles at 3 mA/cm^2 for a total of 1 mAh/cm^2. (**D**) Side-view SEM images of the pristine composite electrode through unwrapping the electrode. (**E**) Side-view SEM images of the composite electrode after cycling under a current density of 3 mA/cm^2 for a total of 1 mAh/cm^2.

electrochemical processes mainly occur in this region because of the electrolyte accessibility inside the porous PE film. Li likely prefers to deposit/strip at the sidewalls of the composite electrode because of the stronger compression on the top surface compared to the sidewalls. This strong compression from the internal pressure of coin cells may impede Li deposition on the top part, thus enhancing the side deposition phenomenon. In addition to the top surface, we studied the morphology of the sidewalls. The composite electrode after cycling was then unwrapped to expose the sidewalls. As presented in Fig. 5E, the sidewall of the composite electrode shows the existence of Li deposits after long-term cycling, which reveals the electrochemical activity of sidewalls. This observation again confirms the side deposition phenomenon, which possibly accounts for the safe and stable battery cycling without dendrite-induced failure. Nevertheless, not all the sidewall surfaces have the same electrochemical activity, which can be verified by the nonuniform spatial distribution of Li deposits across the entire sidewall. The top part of the sidewalls of the composite electrode will probably have higher electrochemical activity and thus more Li deposits than the part deep inside due to limited Li ion diffusion. In addition, because of the spiral structure of this manually rolled Li electrode, the center part of the electrode may behave differently in comparison to the other part. Therefore, the center part of the composite Li electrode after cycling was carefully examined under SEM compared with the outer region, and the corresponding morphologies differ little (fig. S5).

High-capacity cycling of the composite Li electrode

Although the composite electrode exhibits stable and safe cycling under an areal capacity of 1 mAh/cm^2, we proposed a modified version to our original design to satisfy the need for high areal-capacity cycling. The porous PE film is not mechanically strong to sustain the volume/shape variation during high-capacity Li plating/stripping. Thus, rigid crystalline polyimide (PI) films were inserted into the porous PE-containing composite electrode to reinforce the skeleton in the modified design. Crystalline PI can be identified from the x-ray diffraction (XRD) pattern (fig. S6B); three characteristic peaks corresponding to C—N stretching, symmetric C═O stretching, and asymmetric C═O stretching (*26*) can also be identified in the Fourier-transform infrared spectra (FTIR) (fig. S6C). After a simple Li stripping of 5 mAh/cm^2, the unmodified electrode without PI support showed a disordered top surface (fig. S7). The well-defined lamellar structure is destroyed (fig. S7). The collapse of the PE film likely blocks Li ion diffusion and thus increases the charge transfer impedance. However, in the modified design, the electrode structure and shape are preserved to some degree owing to the presence of the rigid PI support (fig. S8). Under high areal capacity of about 5 mAh/cm^2, the composite Li electrode displays excellent structural robustness and cycling stability (fig. S9). Moreover, by adding vinyl carbonate (VC) and fluoroethylene carbonate (FEC) into the electrolyte, the symmetric cell using the spiral Li electrode with rigid PI-reinforced PE matrix can stably cycle for over 50 cycles under a higher current density of 8 mA/cm^2 for a high capacity of 32 mAh/cm^2, which is around 20% utilization of the total Li stored inside (fig. S10).

CONCLUSION

To conclude, in this study, we have developed a new strategy to fabricate a composite Li metal electrode with prestored Li accommodated in a micron-sized ion-conducting matrix. The mesoscale composite electrode displays superior electrochemical performance, as it can cycle stably under high current density with low polarization in both symmetric cell and full-cell configurations. The remarkable performance of the composite electrode originates from the locally reduced current density caused by its relatively high electroactive surface area. The side deposition, where mossy Li deposits on the sidewall of each single Li strip in the composite electrode in addition to the top surface, lowers the risk of Li dendrite penetration. Consequently, the symmetric cell using composite electrodes exhibits no dendrite-induced battery failure for over 200 cycles. Moreover, in the modified version with rigid crystalline PI film as a strong mechanical support, the composite electrode maintains physical integrity and minimal volume fluctuation, thereby achieving stable cycling at a high areal capacity of 32 mAh/cm^2, which is around 20% utilization of the total Li (detailed calculations in fig. S11). To reach an even higher percentage of Li usage, the thickness of the composite Li anode can be further reduced to pair the cathode by using some advanced cutting methods with more precision control. Overall considering the simplicity, low cost, and effectiveness of this design, the mesoscale composite Li electrode constructed via mechanical deformation is expected to contribute significantly to the realization of Li-based energy storage technologies. In addition, the present work will inspire research on other electrode systems as well as other energy technologies.

MATERIALS AND METHODS

Composite electrode fabrication

Li foil (50 μm thick) was purchased from Chongqing Kunyu Co. Ltd. Li foil (380 and 750 μm thick) was purchased from Sigma-Aldrich Co. Ltd. The entire rolling-cutting fabrication process for the composite Li anode was performed inside an argon-filled glove box. First, a strip of Li (length, 160 cm; width, 6 cm; thickness, ~50 μm) was placed on a clean and flat substrate (copper foil in this study). Then, the Li strip was manually smoothed out carefully and slowly until completely flat. Avoid pressing too tightly or else the soft Li strip may stick to the substrate. Afterward, a piece of Celgard PE separator with the same dimension (length, 160 cm; width, 6 cm; thickness, ~12 μm) was put on top of the Li strip to cover it completely. We started from one edge of the strip rolling everything up to the other side, which is similar to closing a scroll. The Li strip and PE separator should be as tight as possible, avoiding too many gaps and folds in between. If the PE separator does not stick to the Li strip, then it will tend to slide and make the rolling process very difficult. As a result, a small amount of liquid electrolyte can be dropped onto the separator to wet it (the total amount of electrolyte in each single cell should be fixed), making the Li strip and PE separator whole. After the rolling, the scroll-like Li-PE composite was then cut into small disks with the thickness of ~1 mm by a razor blade. Because of its ductile nature, the round Li disk may experience some shape deformation during the cutting process, which is fine since the total disk area is about 1 cm^2. Moreover, this cutting process should be done as fast as possible to avoid severe shape deformation. For the modified composite electrode with PI film, three additional pieces of PI films (thickness, ~100 μm) were added in the normal rolling process, such that there are three PI rings for each electrode disk of 1 cm^2. The Li foil purchased from Chongqing Kunyu has an officially certified thickness of 50 to 55 μm according to the manufacturer's specification. We then used an

advanced digital micrometer (Mitutoyo MDC-2 Digital Micrometer, resolution, ~0.0013 mm) to check the thickness, obtaining an average thickness of 56.8 μm after testing over a number of random points. Therefore, all the stated "50-μm Li" in the paper are estimations and noted as 50 μm for convenience. The actual thickness of the Li strip used in this work is in the range of 50 to 60 μm based on our measurements.

Characterization

SEM study of the electrode was conducted using an FEI XL30 Sirion SEM. XRD of the crystalline PI film was performed using an XRD (X'Pert Pro, PANalytical) with Cu Kα radiation. The FTIR spectrum was obtained by a Bruker Vertex 70 FTIR spectrometer. To study the morphology of the cycled electrode, the coin cells were dissembled, and the electrode after cycling was rinsed in pure 1,3-dioxolane (DOL) to remove the Li salts and impurities.

Electrochemistry

Bare Li metal was cut into 1-cm^2 disks by a punch machine (MTI Corporation). Symmetrical MTI type-2032 coin cells were constructed with two identical electrodes inside an Mbraun MB-200B argon-filled glove box; 1 M Li hexafluorophosphate ($LiPF_6$) in cosolvent of ethylene (EC), and diethyl carbonate (DEC) (1:1 vol %) was used as the electrolyte. For high capacity symmetric cycling, 10% FEC and 1% VC were added into the above electrolyte. Symmetric cells were first stripped 32 mAh/cm^2 of Li from one side. Then, this cell was dissembled, and the stripped side was paired with a piece of fresh electrode to form a new cell. Then, this cell was subjected to high capacity cycling. A fixed amount (200 μl) of electrolyte was used in each coin cell to standardize the measurement. Full cells (MTI type-2032) were fabricated with control or composite Li electrodes as the anode and LCO as the cathode. To prepare LCO electrodes, LCO, super-P acetylene black conducting agent, and poly(vinylidene difluoride) binder were mixed at a weight ratio of 90:5:5 in *N*-methyl-2-pyrrolidone (NMP). The mixture was stirred to form a homogeneous slurry. The as-made slurry was pasted on aluminum foil with a total areal capacity of ~0.6 mAh/cm^2. The slurry-coated foil was dried in a vacuum oven at 80°C overnight. Battery testing was performed with a 96-channel battery tester (Arbin Instruments). Electrochemical impedance was measured over the frequency from 0.1 Hz to 200 kHz on an electrochemical workstation (BioLogic Science Instruments, VMP3) at room temperature.

COMSOL simulation

Details of the simulation are presented in fig. S12.

SUPPLEMENTARY MATERIALS

Supplementary material for this article is available at http://advances.sciencemag.org/cgi/content/full/5/3/eaau5655/DC1

Fig. S1. Effect of Li strip thickness on the electrochemical performance of the composite electrode.
Fig. S2. Schematics and the corresponding SEM characterization of dense composite Li electrode with nonporous PE film as the skeleton.
Fig. S3. Li stripping on composite Li electrode with porous and dense PE films.
Fig. S4. Comparison of long-term cycling of symmetric cells.
Fig. S5. Morphology comparison of Li electrode center part with outer region, before and after cycling.
Fig. S6. Characterizations of crystalline PI film.
Fig. S7. Li stripping study of composite Li electrode without crystal PI support.
Fig. S8. Li stripping study of composite Li electrode with rigid PI support.
Fig. S9. Symmetric cycling of control Li electrode, composite Li electrode without PI support, and composite electrode with PI support.
Fig. S10. High-capacity symmetric cycling of various electrodes under a high current density of 8 mA/cm^2 for a total of 32 mAh/cm^2 in an EC/DEC electrolyte containing 10% FEC and 1% VC.
Fig. S11. Detailed information about Li usage for both composite Li and control Li anode and the related calculations.
Fig. S12. The magnified simulation cell geometry in COMSOL.

REFERENCES AND NOTES

1. R. Cao, W. Xu, D. Lv, J. Xiao, J.-G. Zhang, Anodes for rechargeable lithium-sulfur batteries. *Adv. Energy. Mater.* **5**, 1402273 (2015).
2. S. Wei, S. Choudhury, Z. Tu, K. Zhang, L. A. Archer, Electrochemical interphases for high-energy storage using reactive metal anodes. *Acc. Chem. Res.* **51**, 80–88 (2018).
3. W. Xu, J. Wang, F. Ding, X. Chen, E. Nasybulin, Y. Zhang, J.-G. Zhang, Lithium metal anodes for rechargeable batteries. *Energ. Environ. Sci.* **7**, 513–537 (2014).
4. Y. Sun, N. Liu, Y. Cui, Promises and challenges of nanomaterials for lithium-based rechargeable batteries. *Nat. Energy* **1**, 16071 (2016).
5. D. Lin, Y. Liu, Y. Cui, Reviving the lithium metal anode for high-energy batteries. *Nat. Nanotechnol.* **12**, 194–206 (2017).
6. P. G. Bruce, S. A. Freunberger, L. J. Hardwick, J.-M. Tarascon, Li-O_2 and Li-S batteries with high energy storage. *Nat. Mater.* **11**, 19–29 (2011).
7. J. Lu, L. Li, J.-B. Park, Y.-K. Sun, F. Wu, K. Amine, Aprotic and aqueous Li-O_2 batteries. *Chem. Rev.* **114**, 5611–5640 (2014).
8. D. Aurbach, E. Zinigrad, Y. Cohen, H. Teller, A short review of failure mechanisms of lithium metal and lithiated graphite anodes in liquid electrolyte solutions. *Solid State Ion.* **148**, 405–416 (2002).
9. Z.-i. Takehara, Future prospects of the lithium metal anode. *J. Power Sources* **68**, 82–86 (1997).
10. D. Aurbach, E. Zinigrad, H. Teller, P. Dan, Factors which limit the cycle life of rechargeable lithium (metal) batteries. *J. Electrochem. Soc.* **147**, 1274–1279 (2000).
11. F. Wu, Y.-X. Yuan, X.-B. Cheng, Y. Bai, Y. Li, C. Wu, Q. Zhang, Perspectives for restraining harsh lithium dendrite growth: Towards robust lithium metal anodes. *Energ. Storage Mater.* **15**, 148–170 (2018).
12. G. Zheng, S. W. Lee, Z. Liang, H.-W. Lee, K. Yan, H. Yao, H. Wang, W. Li, S. Chu, Y. Cui, Interconnected hollow carbon nanospheres for stable lithium metal anodes. *Nat. Nanotechnol.* **9**, 618–623 (2014).
13. K. Yan, H.-W. Lee, T. Gao, G. Zheng, H. Yao, H. Wang, Z. Lu, Y. Zhou, Z. Liang, Z. Liu, S. Chu, Y. Cui, Ultrathin two-dimensional atomic crystals as stable interfacial layer for improvement of lithium metal anode. *Nano Lett.* **14**, 6016–6022 (2014).
14. J. Qian, W. A. Henderson, W. Xu, P. Bhattacharya, M. Engelhard, O. Borodin, J.-G. Zhang, High rate and stable cycling of lithium metal anode. *Nat. Commun.* **6**, 6362 (2015).
15. Y. Zhang, J. Qian, W. Xu, S. M. Russell, X. Chen, E. Nasybulin, P. Bhattacharya, M. H. Engelhard, D. Mei, R. Cao, F. Ding, A. V. Cresce, K. Xu, J.-G. Zhang, Dendrite-free lithium deposition with self-aligned nanorod structure. *Nano Lett.* **14**, 6889–6896 (2014).
16. X.-B. Cheng, H.-J. Peng, J.-Q. Huang, R. Zhang, C.-Z. Zhao, Q. Zhang, Dual-phase lithium metal anode containing a polysulfide-induced solid electrolyte interphase and nanostructured graphene framework for lithium-sulfur batteries. *ACS Nano* **9**, 6373–6382 (2015).
17. R. Zhang, X.-B. Cheng, C.-Z. Zhao, H.-J. Peng, J.-L. Shi, J.-Q. Huang, J. Wang, F. Wei, Q. Zhang, Conductive nanostructured scaffolds render low local current density to inhibit lithium dendrite growth. *Adv. Mater.* **28**, 2155–2162 (2016).
18. C.-Z. Zhao, X.-B. Cheng, R. Zhang, H.-J. Peng, J.-Q. Huang, R. Ran, Z.-H. Huang, F. Wei, Q. Zhang, Li_2S-based ternary-salt electrolyte for robust lithium metal anode. *Energ. Storage Mater.* **3**, 77–84 (2016).
19. Y. Lu, Z. Tu, L. A. Archer, Stable lithium electrodeposition in liquid and nanoporous solid electrolytes. *Nat. Mater.* **13**, 961–969 (2014).
20. X.-B. Cheng, T.-Z. Hou, R. Zhang, H.-J. Peng, C.-Z. Zhao, J.-Q. Huang, Q. Zhang, Dendrite-free lithium deposition induced by uniformly distributed lithium ions for efficient lithium metal batteries. *Adv. Mater.* **28**, 2888–2895 (2016).
21. K. Yan, Z. Lu, H.-W. Lee, F. Xiong, P.-C. Hsu, Y. Li, J. Zhao, S. Chu, Y. Cui, Selective deposition and stable encapsulation of lithium through heterogeneous seeded growth. *Nat. Energy* **1**, 16010 (2016).
22. K. K. Fu, Y. Gong, J. Dai, A. Gong, X. Han, Y. Yao, C. Wang, Y. Wang, Y. Chen, C. Yan, Y. Li, E. D. Wachsman, L. Hu, Flexible, solid-state, ion-conducting membrane with 3D garnet nanofiber networks for lithium batteries. *Proc. Natl. Acad. Sci. U.S.A.* **113**, 7094–7099 (2016).
23. M. D. Tikekar, S. Choudhury, Z. Tu, L. A. Archer, Design principles for electrolytes and interfaces for stable lithium-metal batteries. *Nat. Energy* **1**, 16114 (2016).
24. Z. Liang, G. Zheng, C. Liu, N. Liu, W. Li, K. Yan, H. Yao, P.-C. Hsu, S. Chu, Y. Cui, Polymer nanofiber-guided uniform lithium deposition for battery electrodes. *Nano Lett.* **15**, 2910–2916 (2015).
25. Z. Liang, D. Lin, J. Zhao, Z. Lu, Y. Liu, C. Liu, Y. Lu, H. Wang, K. Yan, X. Tao, Y. Cui, Composite lithium metal anode by melt infusion of lithium into a 3D conducting scaffold with lithiophilic coating. *Proc. Natl. Acad. Sci. U.S.A.* **113**, 2862–2867 (2016).

26. Y. Liu, D. Lin, Z. Liang, J. Zhao, K. Yan, Y. Cui, Lithium-coated polymeric matrix as a minimum volume-change and dendrite-free lithium metal anode. *Nat. Commun.* **7**, 10992 (2016).
27. D. Lin, Y. Liu, Z. Liang, H.-W. Lee, J. Sun, H. Wang, K. Yan, J. Xie, Y. Cui, Layered reduced graphene oxide with nanoscale interlayer gaps as a stable host for lithium metal anodes. *Nat. Nano* **11**, 626–632 (2016).
28. D. Lin, J. Zhao, J. Sun, H. Yao, Y. Liu, K. Yan, Y. Cui, Three-dimensional stable lithium metal anode with nanoscale lithium islands embedded in ionically conductive solid matrix. *Proc. Natl. Acad. Sci. U.S.A.* **114**, 4613–4618 (2017).
29. A. Brotchie, Li-Metal batteries: Enter the anode matrix. *Nat. Rev. Mater.* **1**, 16022 (2016).
30. C. Jin, O. Sheng, J. Luo, H. Yuan, C. Fang, W. Zhang, H. Huang, Y. Gan, Y. Xia, C. Liang, J. Zhang, X. Tao, 3D lithium metal embedded within lithiophilic porous matrix for stable lithium metal batteries. *Nano Energy* **37**, 177–186 (2017).
31. R. Zhang, X. R. Chen, X. B. Chen, X. B. Cheng, X. Q. Zhang, C. Yan, Q. Zhang, Lithiophilic sites in doped graphene guide uniform lithium nucleation for dendrite-free lithium metal anodes. *Angew. Chem. Int. Ed.* **56**, 7764–7768 (2017).
32. S. Matsuda, Y. Kubo, K. Uosaki, S. Nakanishi, Insulative microfiber 3D matrix as a host material minimizing volume change of the anode of Li metal batteries. *ACS Energ. Lett.* **2**, 924–929 (2017).
33. Q. Li, S. Zhu, Y. Lu, 3D porous Cu current collector/li-metal composite anode for stable lithium-metal batteries. *Adv. Funct. Mater.* **27**, 1606422 (2017).
34. S.-S. Chi, Y. Liu, W.-L. Song, L.-Z. Fan, Q. Zhang, Prestoring lithium into stable 3D nickel foam host as dendrite-free lithium metal anode. *Adv. Funct. Mater.* **27**, 1700348 (2017).
35. R. Zhang, X. Chen, X. Shen, X.-Q. Zhang, X.-R. Chen, X.-B. Cheng, C. Yan, C.-Z. Zhao, Q. Zhang, Coralloid carbon fiber-based composite lithium anode for robust lithium metal batteries. *Joule* **2**, 764–777 (2018).
36. M.-H. Ryou, Y. M. Lee, Y. Lee, M. Winter, P. Bieker, Mechanical surface modification of lithium metal: Towards improved li metal anode performance by directed li plating. *Adv. Funct. Mater.* **25**, 834–841 (2015).
37. I. W. Seong, C. H. Hong, B. K. Kim, W. Y. Yoon, The effects of current density and amount of discharge on dendrite formation in the lithium powder anode electrode. *J. Power Sources* **178**, 769–773 (2008).
38. M.-H. Ryou, D. J. Lee, J.-N. Lee, Y. M. Lee, J.-K. Park, J. W. Choi, Excellent cycle life of lithium-metal anodes in lithium-ion batteries with mussel-inspired polydopamine-coated separators. *Adv. Energy. Mater.* **2**, 645–650 (2012).
39. F. Orsini, A. Du Pasquier, B. Beaudoin, J. M. Tarascon, M. Trentin, N. Langenhuizen, E. De Beer, P. Notten, In situ scanning electron microscopy (SEM) observation of interfaces within plastic lithium batteries. *J. Power Sources* **76**, 19–29 (1998).
40. C. W. Kwon, S. E. Cheon, J. M. Song, H. T. Kim, K. B. Kim, C. B. Shin, S. W. Kim, Characteristics of a lithium-polymer battery based on a lithium powder anode. *J. Power Sources* **93**, 145–150 (2001).
41. W.-S. Kim, W.-Y. Yoon, Observation of dendritic growth on Li powder anode using optical cell. *Electrochim. Acta* **50**, 541–545 (2004).
42. K. Dong, S. Wang, H. Zhang, J. Wu, Preparation and electrochemical performance of sulfur-alumina cathode material for lithium-sulfur batteries. *Mater. Res. Bull.* **48**, 2079–2083 (2013).
43. G. Bieker, M. Winter, P. Bieker, Electrochemical in situ investigations of SEI and dendrite formation on the lithium metal anode. *Phys. Chem. Chem. Phys.* **17**, 8670–8679 (2015).
44. L. Gireaud, S. Grugeon, S. Laruelle, B. Yrieix, J. M. Tarascon, Lithium metal stripping/plating mechanisms studies: A metallurgical approach. *Electrochem. Commun.* **8**, 1639–1649 (2006).
45. D. Wang, W. Zhang, W. Zheng, X. Cui, T. Rojo, Q. Zhang, Towards high-safe lithium metal anodes: Suppressing lithium dendrites via tuning surface energy. *Adv. Sci.* **4**, 1600168 (2017).
46. J. Zheng, P. Yan, D. Mei, M. H. Engelhard, S. S. Cartmell, B. J. Polzin, C. Wang, J.-G. Zhang, W. Xu, Highly stable operation of lithium metal batteries enabled by the formation of a transient high-concentration electrolyte layer. *Adv. Energy. Mater.* **6**, 1502151 (2016).

Acknowledgments

Funding: Part of this work was performed at the Stanford Nano Shared Facilities. This work was supported by the Assistant Secretary for Energy Efficiency and Renewable Energy, Office of Vehicle Technologies of the U.S. Department of Energy, under the Battery Materials Research program and the Battery 500 Consortium program. A.P. acknowledges the support from the U.S. Department of Defense through the National Defense Science and Engineering Graduate Fellowship (NDSEG) Program and from Stanford University through the Stanford Graduate Fellowship (SGF) Program. **Author contributions:** Y.C., Z.L., and K.Y. conceived the idea. Z.L. performed the experiments. G.Z. purchased the Li strips. A.P. conducted simulations. F.S. conducted the FTIR experiments. Z.L. and Y.C. co-wrote the paper. J.Z., Y.S., J.X., Y. Li, Y. Liu, D.L., K.L., Hansen Wang, Hongxia Wang, and Y. Lu, provided valuable discussions and thoughts. All authors discussed the results and commented on the manuscript. **Competing interests:** The authors declare that they have no competing interests. **Data and materials availability:** All data needed to evaluate the conclusions in the paper are present in the paper and/or the Supplementary Materials. Additional data related to this paper may be requested from the authors.

Submitted 26 June 2018
Accepted 29 January 2019
Published 15 March 2019
10.1126/sciadv.aau5655

Citation: Z. Liang, K. Yan, G. Zhou, A. Pei, J. Zhao, Y. Sun, J. Xie, Y. Li, F. Shi, Y. Liu, D. Lin, K. Liu, H. Wang, H. Wang, Y. Lu, Y. Cui, Composite lithium electrode with mesoscale skeleton via simple mechanical deformation. *Sci. Adv.* **5**, eaau5655 (2019).

Composite lithium electrode with mesoscale skeleton via simple mechanical deformation

Zheng Liang, Kai Yan, Guangmin Zhou, Allen Pei, Jie Zhao, Yongming Sun, Jin Xie, Yanbin Li, Feifei Shi, Yayuan Liu, Dingchang Lin, Kai Liu, Hansen Wang, Hongxia Wang, Yingying Lu and Yi Cui

Sci Adv **5** (3), eaau5655.
DOI: 10.1126/sciadv.aau5655